Microburst Scale Size Derived from Multiple Bounces of a Microburst Simultaneously Observed with the FIREBIRD-II CubeSats

Mykhaylo Shumko[1], John Sample[1], Arlo Johnson[1], Bern Blake[2], Alex Crew[3], Harlan Spence[4], David Klumpar[1], Oleksiy Agapitov[5], Matthew Handley[1]

[1]Department of Physics, Montana State University, Bozeman, Montana, USA
[2]Space Science Applications Laboratory, The Aerospace Corporation, Los Angeles, California, USA
[3]The Johns Hopkins University Applied Physics Laboratory LLC, Laurel, Maryland, USA
[4]Institute for the Study of Earth, Oceans, and Space, University of New Hampshire, Durham, New Hampshire, USA
[5]Space Sciences Laboratory, UC Berkeley, Berkeley, California, USA

Key Points:

- The lat/lon scale sizes at LEO were 28.8 ± 0.8 km and 50.8 ± 11.4 km, respectively.
- (Replaced: ~~Magnetic equator scale sizes are similar to the whistler-mode chorus source scale.~~ replaced with: Deduced lower bound equatorial scale size is similar to the whistler-mode chorus source scale.)

Corresponding author: Mykhaylo Shumko, msshumko@gmail.com

Abstract

The FIREBIRD-II CubeSats simultaneously observed a large microburst with multiple bounces on February 2nd, 2015 during a small storm. This is the first such microburst observed by two spacecraft, and it sheds light on its spatial scale sizes and bounce periods. Its lower bound latitudinal scale size was 28.8 ± 0.8 km and the longitudinal scale size was 50.8 ± 11.4 km in low earth orbit. Using the Tsyganenko 1989 magnetic field model, these scale sizes were mapped to the magnetic equator to get the radial and azimuthal scale sizes of at least 504 ± 14 km and 530 ± 119 km, respectively. These (Added: lower bound) equatorial scale sizes are similar to (Deleted: ~~the~~) whistler-mode chorus wave source scale sizes, which (Deleted: ~~further~~) (Replaced: ~~support~~ replaced with: supports) the hypothesis that microbursts are a product of (Replaced: ~~whistler-mode chorus waves scattering radiation belt electrons~~ replaced with: electron scattering by chorus waves). Lastly, the electron bounce period from the subsequent bounces was calculated and compared to analytical and numerical bounce times to validate numerous magnetic field models.

1 Introduction

The dynamics of radiation belt electrons are complex, and are driven by competition between source and loss processes. A few possible loss processes are radial diffusion [*Shprits and Thorne*, 2004], magnetopause shadowing [*Ukhorskiy et al.*, 2006], and pitch angle diffusion [*Selesnick et al.*, 2003; *Abel and Thorne*, 1998] due to plasma wave and Coulomb scattering. As described in [*Millan and Thorne*, 2007; *Thorne*, 2010] and references contained within, there are a variety of waves that cause pitch angle scattering, including electromagnetic ion cyclotron waves, plasmaspheric hiss, and whistler-mode chorus. Whistler-mode chorus predominantly occurs in the dawn sector [*Li et al.*, 2009] where it accelerates electrons with large equatorial pitch angles and scatters electrons with small equatorial pitch angles [*Horne and Thorne*, 2003]. (Replaced: ~~It is currently believed that chorus waves are responsible for microbursts, an intense increases in electron precipitation flux lasting ~ 100 *ms*.~~ replaced with: Some of these electrons may be impulsively scattered into the loss cone. This sudden increase (duration ≈100 ms) in precipitating electron flux is believed to be caused by scattering with whistler-mode chorus waves [e.g. *Thorne et al.*, 2005; *Breneman et al.*, 2017].)

Microbursts were first termed by *Anderson and Milton* [1964] who used high altitude balloon observations of bremsstrahlung X-rays emitted (Replaced: ~~from scattered microburst~~

~~electrons in the atmosphere~~ replaced with: from scattered electrons impacting the atmosphere). Since then, microbursts have routinely been observed with other balloon missions [*Parks*, 1967; *Woodger et al.*, 2015; *Anderson et al.*, 2017]. (Added: Relativistic microbursts have not been observed by high altitude balloons in the dawn sector [*Millan et al.*, 2002], which may be caused by a pitch angle anisotropy of relativistic microbursts due to relatively weaker pitch angle scattering of relativistic electrons by chorus [*Lee et al.*, 2012].) (Replaced: ~~and in~~ replaced with: Microbursts have also been observed in) low earth orbit (LEO) with, e.g. (Added: the) SAMPEX > 1 MeV (Deleted: ~~energy~~) channel [*Nakamura et al.*, 1995, 2000; *Blake et al.*, 1996; *Lorentzen et al.*, 2001a,b; *O'Brien et al.*, 2003, 2004; *Blum et al.*, 2015] and FIREBIRD-II with its > 200 keV energy channels [*Crew et al.*, 2016; *Breneman et al.*, 2017]. (Deleted: ~~Similar to chorus waves,~~) Microbursts (Added: and chorus waves) predominantly occur in the dawn sector, (Added: are bursty [*Lorentzen et al.*, 2001b], and observationally *Breneman et al.* [2017] directly linked microbursts scattered by whistler-mode chorus). Understanding microburst precipitation is important to radiation belt dynamics since they have been modeled and empirically estimated to deplete the relativistic electron population of the outer radiation belt on time scales of hours to a few days [*O'Brien et al.*, 2004; *Thorne et al.*, 2005; *Shprits et al.*, 2007; *Breneman et al.*, 2017].

An important parameter in the estimation of instantaneous radiation belt electron losses due to microbursts is their scale size. *Parks* [1967] used balloon measurements of bremsstrahlung X-rays to estimate the scale size of predominantly low energy microbursts as 40 ± 14 km. In *Blake et al.* [1996] a microburst with multiple bounces (Deleted: ~~was~~) observed (Replaced: ~~with~~ replaced with: by) SAMPEX, was estimated to have a latitudinal scale size of "at least a few tens of kilometers", and (Added: they) concluded that typically (Replaced: ~~they~~ replaced with: microbursts) are less than a few tens of electron gyroradii in size (Added: (at L = 5 at LEO, the gyroradii of 1 MeV electrons is on the order of 100 m)). *Dietrich et al.* [2010] used SAMPEX along with ground-based very low frequency stations to conclude that microbursts have scale sizes less than 4 km.

Since February 1st, 2015, microbursts have been observed by FIREBIRD-II, a pair of CubeSats in LEO. (Replaced: ~~On February 2nd, 2015, [*Crew et al., 2016*] reported~~ replaced with: Soon after launch, when the two FIREBIRD-II spacecraft were at close range,) a microburst with a scale size greater than 11 km was observed [*Crew et al.*, 2016]. On the same day, a microburst with multiple bounces was simultaneously observed on both spacecraft. The microburst decay was observed over (Replaced: ~~the~~ replaced with: a) period of a

few seconds, while the spacecraft were traveling predominantly in latitude. (Replaced: ~~This analysis~~ replaced with: The analysis in this paper uses) FIREBIRD-II to resolve the spatial and temporal properties of the first microburst with multiple bounces observed with two spacecraft. The rest of this paper is organized as follows: in section 2, the spacecraft and the microburst observation will be introduced. In section 3, the methodology of the spacecraft time and position correction, the microburst latitudinal and longitudinal scale sizes in LEO and the magnetic equator, and electron bounce period will be explained. Lastly, in section 4, these results will be tied to the current empirical and theoretical understanding of microbursts and their connection to whistler-mode chorus scales.

2 Spacecraft and Observation

FIREBIRD-II is an identically-instrumented pair of 1.5U CubeSats (Replaced: ~~(FU3 and FU4)~~ replaced with: (15 cm x 10 cm x 10 cm) that are termed Flight Unit 3 (FU3) and Flight Unit 4 (FU4) and were) launched on January 31st, 2015. Their orbit has an apogee of 632 km, perigee of 433 km, and 99° inclination [*Crew et al.*, 2016]. FU3 and FU4 are flying in a string of pearls configuration with FU4 ahead, to resolve the space-time ambiguity inherent to single spacecraft missions such as SAMPEX. Each FIREBIRD-II unit has a collimated and a surface solid state detector with complementary fields of view of 54° and 90°, (Added: respectively). They are observing electron precipitation in six energy channels from $\sim$ 230 keV to $>$ 1 MeV. The adjustable sampling rate is 18.75 ms by default and can be at a fast as 12.5 ms.

On February 2nd, 2015 at 06:12:53 UT, a microburst and subsequent bounces were observed simultaneously on both spacecraft. Figure 1 shows the (Added: High Resolution (HiRes)) electron flux (Deleted: ~~data (HiRes))~~of the microburst, sampled at 18.75 ms. Five peaks were observed on both spacecraft. On the collimated detector, the microburst was seen up to the fourth energy channel (555 - 771 keV), while on the surface detector it was observed up to the fifth energy channel (683 - 950 keV). Only FU3 has a functioning surface detector, thus only data from the lowest four energy channels of the collimated detectors was used for this analysis. Furthermore, since FU4's 5th peak in the fourth energy channel was buried in Poisson noise, only the first four peaks were used in the spatial scale analysis.

(Replaced: ~~The earliest peak was not dispersed, and subsequent peaks showed dispersion, which implies that this was a single microburst with subsequent decaying bounces.~~ replaced

with: From the black vertical black bars in Fig. 1, the first peak does not appear to be dispersed, and subsequent peaks show dispersion consistent across energy channels. This dispersion signature and amplitude decay implies that the first peak was observed soon after the electrons were scattered, followed by decaying bounces.) At this time, the spacecraft was above Sweden, latitude = 63°N, longitude = 15°E, altitude = 650 km, at the eastern edge of the bounce loss cone (BLC). For this analysis, the BLC is defined as the region where locally mirroring electrons will mirror at an altitude less than 100 km in the opposite hemisphere, and could be lost due to collisions in the atmosphere [*Abel and Thorne*, 1998]. (Added: This unique observation of returning bounces was possible since FIREBIRD-II was at the eastern edge of the BLC; any background electron flux that was in the drift loss cone was recently lost to the South Atlantic Anomaly. In the drift loss cone, any returning bounces from microbursts will be quickly hidden in the background electron flux.) For locally mirroring electrons, the mirror point in the opposite hemisphere was calculated to be 95 km using the Tsyganenko 1989 (T89) magnetic field model [*Tsyganenko*, 1989] with the IRBEM-Lib library. (Added: From the analysis done by *Fang et al.* [2010], the peak total ionization rate in the atmosphere for 100 keV electrons is around 80 km altitude, while 1 MeV electrons have a peak total ionization rate round 60 km altitude, so it is expected that a fraction of the microburst electrons will survive each encounter with the atmosphere.) (Replaced: ~~Roughly~~ replaced with: By plotting the peak flux as a function of bounce, it was found that) 40 - 60 % of the microburst electrons were lost (Replaced: ~~at each bounce~~ replaced with: on the first bounce), (Added: similar to the 33% loss per bounce observed for a bouncing microburst observed by SAMPEX [*Thorne et al.*, 2005]).

The geomagnetic conditions at the time were Kp = 4, (Added: AE ≈ 400 nT) and DST = -44 nT, during the transition between the main and recovery phases (Added: of a geomagnetic storm). (Replaced: ~~Using the spacecraft location and geomagnetic conditions, the geomagnetic location at this time was McIlwain L = 4.7, MLT = 8.3, calculated with the T89 model.~~ replaced with: At the time of the microburst, FIREBIRD-II was at McIlwain L = 4.7 and MLT = 8.3, calculated with the T89 model.)

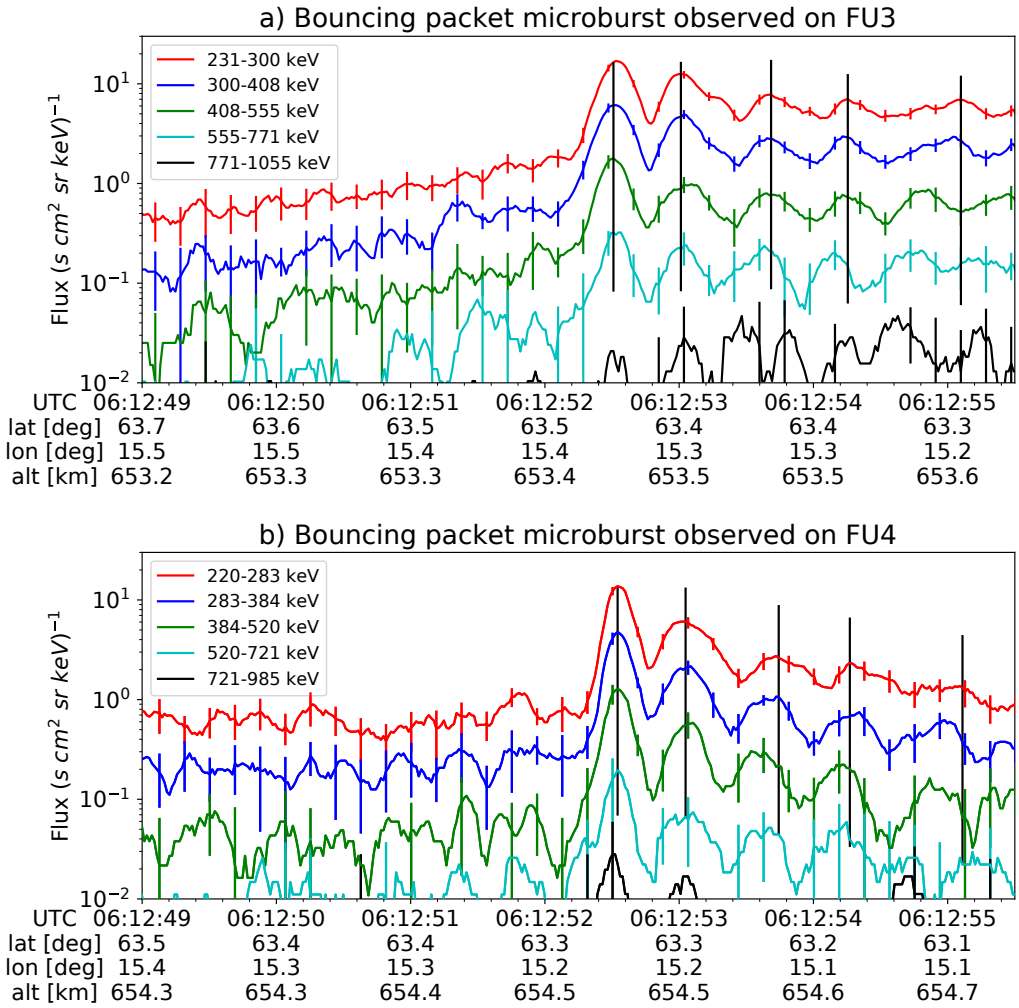

Figure 1. HiRes data of the microburst observed at February 2nd, 2015 at 06:12:53 UT, smoothed with a 150 ms rolling average. The subsequent bounces showed some energy dispersion. As discussed in section 3 a time correction of -2.28 s was applied to FU3. While the flux from five energy channels is shown, only channels with reasonable counting statistics were used for the spatial scale analysis. Vertical colored bars show the $\sqrt{N}$ error every 10th data point and vertical black bars are lined up with the peaks in the 220-283 keV energy channel to help identify dispersion.

3 Analysis

3.1 Time and position correction

(Replaced: ~~At the beginning of the FIREBIRD-II mission, their clocks were not synchronized and there was uncertainty in their separation. The approach to calculate their relative clock difference δt_c, is a cross-correlation time lag analysis on temporal events that are occurred simultaneously, e.g. a train of identical microbursts seen on both spacecraft on the same day as the microburst in this case study.~~ replaced with: At the beginning of the FIREBIRD-II mission, there were two issues with the spacecraft timing and position; their clocks were not synchronized and there was uncertainty in their separation. The approach to solve the former problem was to calculate the relative clock difference δt_c between the two spacecraft. The clock difference was calculated via a cross-correlation time lag analysis on trains of microbursts that hit both spacecraft simultaneously. A time lag can be calculated since the amplitudes and repetition rate of individual microbursts in these trains is unique (see Figs. S1-S4).)

(Added: To correct FIREBIRD-II's relative clock difference,) four time periods with coincident microbursts were hand-picked on February 2nd, 2015. (Deleted: ~~for this analysis~~). The clock difference from the simultaneous microbursts was linearly fit to account for the (Added: relative) clock drift (≈20 ms/hour at this time), (Replaced: ~~and it was~~ replaced with: giving a value of) $\delta t_c = 2.28 \pm 0.12$ s at the time of the microburst (Added: analyzed here). This time shift was applied to the HiRes data in Fig. 1. (Replaced: ~~To independently confirm the clock difference, it~~ replaced with: The clock difference) was also (Added: independently) calculated using the time stamps of the FIREBIRD-II telemetry beacons during operational passes. Since they had a common time reference, the ground station computer, a time difference $\delta t_c = 2.45^{+0.51}_{-0.98}$ s was derived.

To calculate (Replaced: ~~their~~ replaced with: the spacecraft) separation, the data was first corrected for the clock difference, and the same cross-correlation time lag analysis was applied to (Replaced: ~~spatial events that~~ replaced with: events that are assumed to be stationary (see Figs. S5 and S6)). (Replaced: ~~This time lag, δt_d for spatial events is the time it takes the trailing satellite to move to the leading satellite's position.~~ replaced with: The time lag between spatial events, δt_d is the time difference between when the leading satellite observed a stationary spatial feature, to when the trailing satellite observed the same stationary spatial feature.) This analysis yielded a time lag of $\delta t_d = 2.64 \pm 0.12$ s. In the last step

in the separation calculation, their velocity needed to be calculated using a Two Line Element (TLE), a data format containing the Keplerian elements for orbit propagation. With the TLE derived spacecraft velocity, $v = 7.57\ km/s$, the calculated spacecraft separation was, $d = 19.9 \pm 0.9\ km$.

An independent method to confirm the spacecraft separation was developed. The separation was calculated using TLEs. The TLE released for February 2nd, was anomalous and was not used. Instead, seven TLEs released up to five days after the microburst event were backpropagated, using the SGP-4 algorithm [*Hoots and Roehrich*, 1980] (Added: that calculates orbital state vectors with perturbations such as Earth's atmosphere, as well as gravitational effects from the moon and sun). Then the predicted spacecraft separations at the time of the microburst event were averaged to derive a separation of $d = 18.4 \pm 1.5$ km. These two methods give similar results, which imply that the stationary event assumption used in the cross-correlation time lag analysis is (Replaced: ~~a reasonable assumption~~ replaced with: reasonable).

3.2 Microburst Scale Sizes

(Replaced: ~~Using the event and orbit topology shown in Fig. 2 and error propagated from the cross-correlation derived spacecraft separation, the latitudinal scale size is greater than 28.8 ± 0.8 km. This scale size is represented by the latitudinal extent of the rectangles in Fig. 2.~~ replaced with: With the spacecraft orbit, corrected separation, and timeseries from Fig. 1, a map in longitude-latitude was made and is shown in Fig. 2. The locations where FU3 saw peaks 1-5 and where FU4 saw peaks 1-4 are shown as P1-5 and P1-4, respectively. The lower bound on the latitudinal extent of the microburst was the difference in latitude between P1 on FU3 and P4 on FU4 and was found to be 28.8 ± 0.8 km. The uncertainty was estimated from the spacecraft separation uncertainty calculated in section 3.1. This scale size is the largest observed by FIREBIRD-II.)

(Replaced: ~~Since magnetospheric electrons drift eastward and were seen for multiple bounces, it is possible to calculate the longitudinal scale size of the microburst.~~ replaced with: To calculate the longitudinal scale size of the microburst, it is assumed that electrons observed in the last bounce by FIREBIRD-II must have begun drifting when the initial microburst was observed, to the west of the spacecraft. Following geometrical arguments, the distance that electrons drift azimuthally in a single bounce is a product of the circumfer-

ence of the drift shell foot point, and the fraction of the total drift orbit traversed in a single bounce and is) given by,

$$d_{az} = 2\pi(R_E + A)\cos(\lambda)\frac{t_b}{< T_d >} \tag{1}$$

where R_E is the Earth's radius, A is the spacecraft altitude, λ is the magnetic latitude, t_b is the electron bounce period, and $< T_d >$ is the electron drift period. *Parks* [2003] derived $< T_d >$ to be,

$$< T_d > \approx \begin{cases} 43.8/(L \cdot E) & \text{if } \alpha_0 = 90° \\ 62.7/(L \cdot E) & \text{if } \alpha_0 = 0° \end{cases} \tag{2}$$

where E is the electron energy in MeV, L is the L shell, and α_0 is the equatorial pitch angle. (Replaced: ~~The valid limit for this analysis is $\alpha_0 = 0°$ since electrons mirroring at FIREBIRD-II have $\alpha_0 \approx 3.7°$.~~ replaced with: Electrons mirroring at FIREBIRD-II have $\alpha_0 \approx 3.7°$ and so the $\alpha_0 = 0°$ limit was used.)

The microburst's longitudinal scale size (Replaced: ~~was~~ replaced with: is defined as) the furthest distance that its electrons drifted east and were last seen. This was calculated with $D_{az} = n\, d_{az}$ where n is the number of bounces observed. The stars with energy labels in Fig. 2 represent the locations of electrons with that energy when the microburst was seen at (Replaced: ~~the first peak (P1)~~ replaced with: P1), and drifted eastward to be last seen at P5 for FU3 and P4 for FU4. Using this methodology, the longitudinal scale size was greater than 38.5 ± 8.8 km for the 555 keV electrons and greater than 50.8 ± 11.4 km for the 771 keV electrons, shown with the red dashed box in Fig. 2. (Added: The uncertainty was estimated by propagating the uncertainty in the spacecraft separation through Eq. 1).

The longitudinal and latitudinal scale sizes (Added: and their uncertainties) at LEO were mapped to the magnetic equator using the T89 magnetic field model. The radial scale size (latitudinal scale mapped from LEO) is greater than 504 ± 14 km and azimuthal scale size (longitudinal scale mapped from LEO) of 555 keV electrons is greater than 451 ± 103 km and of 771 keV electrons is greater than 530 ± 119 km.

3.3 Electron Bounce Period

Lastly, the observed bounce period, t_b as a function of energy was calculated. To calculate the observed t_b and uncertainties, the raw HiRes flux was baseline-subtracted and fitted. The baseline flux (Added: used in this analysis) is (Replaced: ~~defined~~ replaced with:

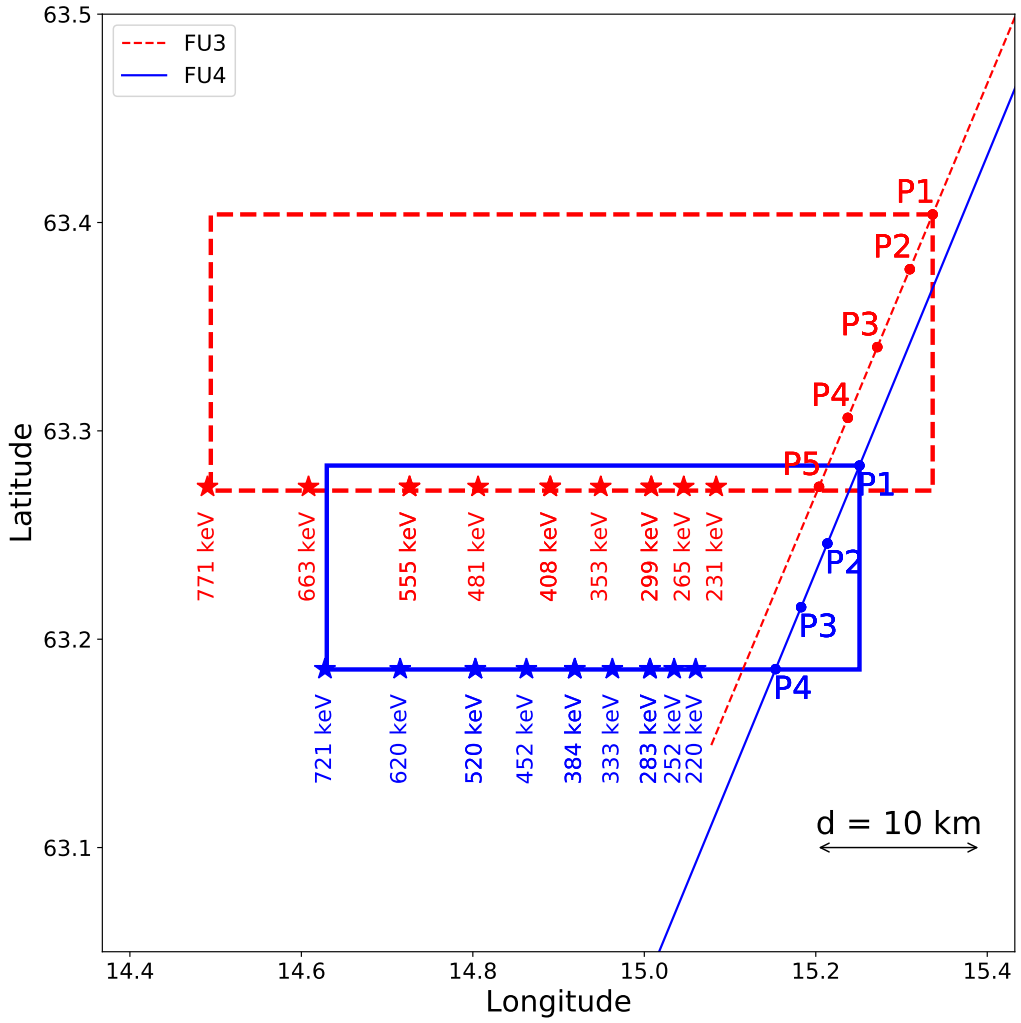

Figure 2. The topology of the FIREBIRD-II orbit and the multiple bounces of the microburst projected onto latitude and longitude with axis scaled to equal distance. Attributes relating to FU3 shown in red dashed lines, and FU4 with blue solid lines. The spacecraft path is shown with the diagonal lines, starting at the upper right corner. The labels P1-4 for FU4 and P1-5 for FU3 indicate where the spacecraft were when the N^{th} peak was seen in the lowest energy channel in the HiRes data. The stars with the accompanying energy labels represent the locations of the electrons with that energy that started at time of P1, and were seen at the last peak on each spacecraft. The rectangles represent the lower bound of the microburst scale size, assuming that the majority of the electrons were in the upper boundary of energy channel 4.

given) in *O'Brien et al.* [2004] as the flux at the 10th percentile over a specified time interval, (Replaced: ~~half second for this analysis~~ replaced with: which in this analysis was taken to be 0.5 seconds). The flux was fitted with (Replaced: ~~multiple superposed~~ replaced with: a superposition of) Gaussians (Added: for each energy channel). The flux uncertainty is from the Poisson errors of microburst and baseline fluxes summed in quadrature. Using the fit parameters, the mean t_b for the lowest four energy channels was calculated and shown in Fig. 3 with green and purple rectangles.

The bounces observed with FU3 (Replaced: ~~were biased~~ replaced with: had in-channel dispersion) to earlier times in the lowest two energy channels. This hints at the underlying distribution of electron flux within those energy channels. (Replaced: ~~and suggests that there were more electrons at the higher energy end.~~ replaced with: If FIREBIRD-II had finer energy resolution, the peak flux would be towards the upper end of the first energy channel.) A Gaussian fit cannot account for this (Replaced: ~~bias~~ replaced with: in-channel dispersion), and as a first order correction, minima between peaks was used to calculate t_b, and is shown in Fig. 3 with blue rectangles. (Added: The observed energy-dependent dispersion shown in Fig. 3 is consistent with higher energy peaks returning sooner. This dispersion consistency further supports the assumption that the subsequent peaks are bounces, and not a train of microbursts scattered by bouncing chorus.)

Superposed on Fig. 3, are t_b curves for various models including an analytical solution (Added: in a dipole) [*Schulz and Lanzerotti*, 1974], and numerical models: T89, Tsyganenko 2004 (T04) [*Tsyganenko and Sitnov*, 2005], and Olson & Pfitzer Quiet [*Olson and Pfitzer*, 1982]. The numerical t_b curves were calculated using a Python wrapper for IRBEM-Lib. It traces the magnetic field line between mirror points, to calculate t_b assuming conservation of energy and the first adiabatic invariant for electrons mirroring at FIREBIRD-II. (Added: A discrepancy of ≈20% between the observed bounce periods derived from the fits and the models is seen at the lower energies, and is reduced at the higher energy channels. The low energy discrepancy is removed by using the minima to calculate t_b for the < 555 keV peaks. Across all but one energy channel, the T04 model has the largest discrepancy compared to other models.)

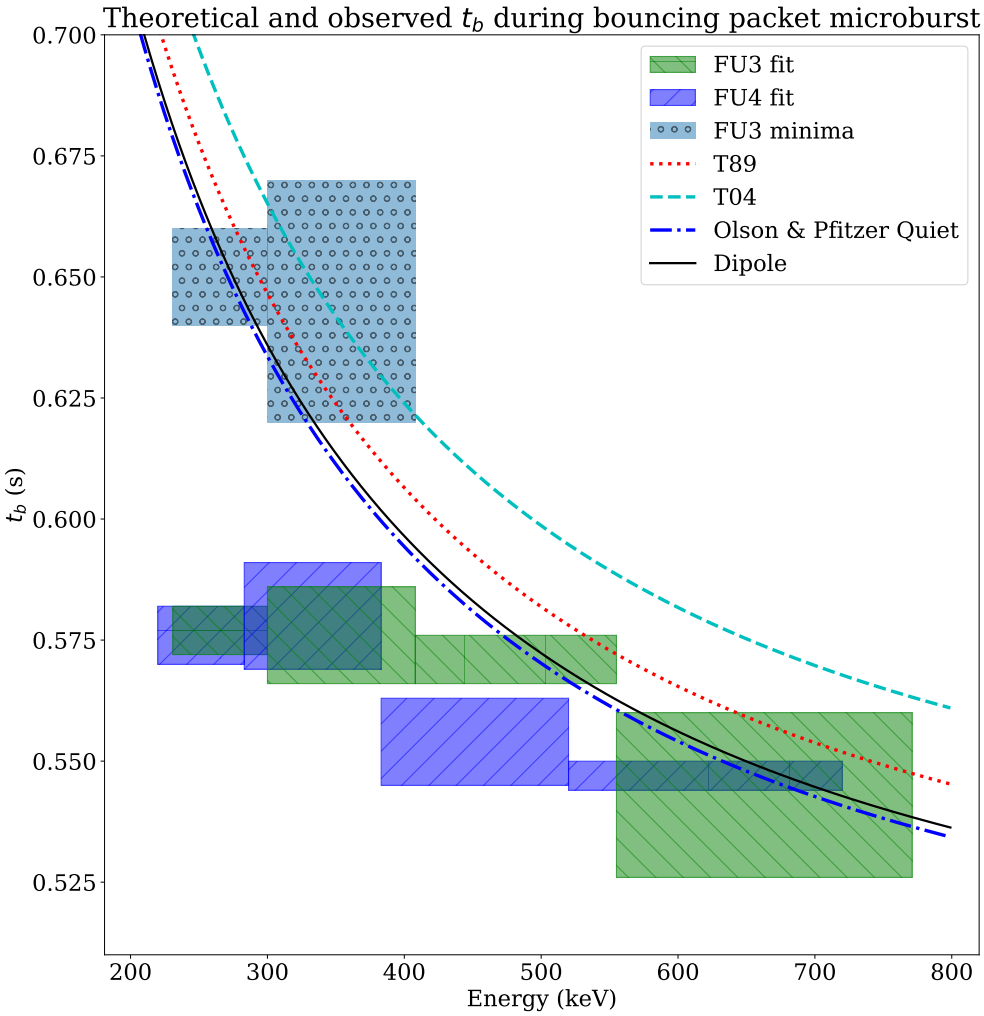

Figure 3. Observed and theoretical t_b for electrons of energies from 200 to 770 keV. The solid black line is t_b in a dipole magnetic field, derived in *Schulz and Lanzerotti* [1974]. The red and cyan dashed lines are the t_b derived using the T89, and T04 magnetic field models with IRBEM. Lastly, the blue dashed curve is the t_b derived using the Olson & Pfitzer Quiet model. The green and purple rectangles represent the observed t_b for FU3 and FU4 using a Gaussian fit, respectively. The blue rectangles represent the observed t_b calculated with the minima between the bounces. The width of the boxes represent the width of those energy channels, and the height represents the uncertainty from the fit.

4 Discussion

(Replaced: ~~The scale sizes reported in section 3.2 were a lower bound.~~ replaced with: The twin FIREBIRD-II CubeSats have enabled a direct estimate of the lower bound scale size of a large microburst.) (Replaced: ~~They were~~ replaced with: This microburst is) larger than the latitudinal scale sizes (Added: of > 1 MeV microbursts) reported in *Blake et al.* [1996], and similar to the scale sizes (Replaced: ~~reported in~~ replaced with: of > 15 keV microbursts observed with a high altitude balloon) [*Parks*, 1967]. Furthermore, the latitudinal scale size in this study was roughly ~ 2.6 times larger than other simultaneous microbursts reported in *Crew et al.* [2016] and ~ 10 times larger than than reported in *Dietrich et al.* [2010]. No energy dependence on the scale size was observed.

(Replaced: ~~From section 3.2, the microburst scale size at the magnetic equator was similar to the whistler-mode chorus source scale sizes reported in [*Agapitov et al.*, 2011, 2017]. In *Agapitov et al.* 2011, chorus source scale scales of ~ 600 *km* were observed by CLUSTER at $L \sim 4.5$. In *Agapitov et al.* 2017, The Van Allen Probes were used to measure source scale sizes of ~ 500 and ~ 800 km for upper and lower band chorus, respectively. Using the evidence from this analysis, this microburst was most likely scattered by a whistler-mode chorus.~~ replaced with: The microburst scale size obtained in Section 3.2 and scaled to the geomagnetic equator can be compared with the scales of chorus waves presumably responsible for the rapid burst electron precipitation. Early direct estimates of the chorus source scales were made by the coordinated measurement by ISEE-1, 2. The wave power correlation scale was estimated to be about several hundred kilometers across the background magnetic field [*Gurnett et al.*, 1979]. Later, *Santolik et al.* [2003] determined the correlation lengths of chorus-type whistler waves based on multipoint CLUSTER WBD measurements near the chorus source region during the magnetic storm of 18 April 2002 at L shell about 4 (in the region around the plasmapause). Correlation scales were found to be around 100 km from the dependence of the chorus wave amplitude correlation coefficient on the distance between the CLUSTER spacecraft. *Agapitov et al.* [2010, 2011, 2017] recently showed that the spatial extent of chorus source region can be larger: from 600 km in the outer radiation belt to more than 1000 km in the outer magnetosphere. The lower bound azimuthal and latitudinal scales obtained in Section 3.2 and scaled to the magnetic equator, were similar to the whistler-mode chorus source scale sizes reported in *Agapitov et al.* [2011, 2017]. No wave measurements from nearby spacecraft were available at this time to confirm the presence of chorus. Nevertheless, since AE ~ 400 nT at this time, relatively strong chorus waves were

statistially more likely to occur [*Li et al.*, 2009]. This microburst was likely scatter by chorus, similar to the conclusions made by e.g. *Lorentzen et al.* [2001a]; *O'Brien et al.* [2003]; *Breneman et al.* [2017].)

Using the fit parameters from section 3.3, the exponential E-folding energy, E_0 was calculated to be $E_0 \sim 100\ keV$. This is similar to the results in *Lee et al.* [2005] who used STSAT-1 and *Datta et al.* [1997] who used a sounding rocket. It is soft for a typical microburst observed with FIREBIRD-II. There was no statistically significant change in E_0 for subsequent bounces.

(Deleted: ~~Lastly, the fitted, high energy t_b shown in Fig. 3 agrees to most models but has the largest discrepancy at lower energies. This discrepancy is removed by using the minima to calculate t_b for the < 555 keV peaks.~~)

5 Conclusions

This was a first observation of a large microburst with multiple bounces (Replaced: ~~by two spaceecraft~~ replaced with: made possible by the twin FIREBIRD-II CubeSats). Its lower bound LEO latitudinal and longitudinal scale sizes of 28.8 ± 0.8 km and 50.8 ± 11.4 km make it one of the largest observed. No energy dependence on the scale size was observed. Furthermore, its lower bound LEO scale sizes mapped to the magnetic equator were 504 ± 14 km radially and 530 ± 119 km azimuthally. (Replaced: ~~similar to the whistler-mode chorus source region scale size reported in previous literature. The Gaussian fitted and theoretical bounce periods agree at high energies, but disagree by as much as ~ 20% at the lowest energies that FIREBIRD-II observes. This is partially due to the bias to earlier times in the peaks for the two lowest energy channels, and it hints at the underlying energy-dependent electron flux spectra. By using the minima method to calculate t_b, there is better agreement for those energy channels.~~ replaced with: The bounce periods calculated with the Gaussian fit and minima methods are in good agreement with the theoretical bounce periods, confirming that the energy-dependent dispersion was due to bouncing.) The similarity of the microburst and chorus source region scale sizes, as well as magnetospheric location and condition, support the idea that microbursts are scattered by whistler-mode chorus.

Acknowledgments

This work was made possible with help from the FIREBIRD team, and the members of the Space Sciences and Engineering Laboratory at Montana State University for their hard work to make this mission a success. In addition, I acknowledge Drew Turner for his suggestions regarding the bounce period calculations. The FIREBIRD-II data are available at http://solar.physics.montana.edu/FIREBIRD_II/. This material is based upon work at Montana State University supported by the National Science Foundation under Grant Numbers 0838034 and 1339414.

References

Abel, B., and R. M. Thorne (1998), Electron scattering loss in earth's inner magnetosphere: 1. dominant physical processes, *Journal of Geophysical Research: Space Physics*, *103*(A2), 2385–2396.

Agapitov, O., V. Krasnoselskikh, Y. Zaliznyak, V. Angelopoulos, O. Le Contel, and G. Rolland (2010), Chorus source region localization in the earth's outer magnetosphere using themis measurements, *Annales Geophysicae*, *28*(6), 1377–1386, doi:10.5194/angeo-28-1377-2010.

Agapitov, O., V. Krasnoselskikh, T. Dudok de Wit, Y. Khotyaintsev, J. S. Pickett, O. Santolik, and G. Rolland (2011), Multispacecraft observations of chorus emissions as a tool for the plasma density fluctuations' remote sensing, *Journal of Geophysical Research: Space Physics*, *116*(A9), n/a–n/a, doi:10.1029/2011JA016540, a09222.

Agapitov, O., L. W. Blum, F. S. Mozer, J. W. Bonnell, and J. Wygant (2017), Chorus whistler wave source scales as determined from multipoint van allen probe measurements, *Geophysical Research Letters*, pp. n/a–n/a, doi:10.1002/2017GL072701, 2017GL072701.

Anderson, B., S. Shekhar, R. Millan, A. Crew, H. Spence, D. Klumpar, J. Blake, T. O'Brien, and D. Turner (2017), Spatial scale and duration of one microburst region on 13 august 2015, *Journal of Geophysical Research: Space Physics*.

Anderson, K. A., and D. W. Milton (1964), Balloon observations of x rays in the auroral zone: 3. high time resolution studies, *Journal of Geophysical Research*, *69*(21), 4457–4479, doi:10.1029/JZ069i021p04457.

Blake, J., M. Looper, D. Baker, R. Nakamura, B. Klecker, and D. Hovestadt (1996), New high temporal and spatial resolution measurements by sampex of the precipitation of relativistic electrons, *Advances in Space Research*, *18*(8), 171 – 186, doi:

http://dx.doi.org/10.1016/0273-1177(95)00969-8.

Blum, L., X. Li, and M. Denton (2015), Rapid mev electron precipitation as observed by sampex/hilt during high-speed stream-driven storms, *Journal of Geophysical Research: Space Physics*, *120*(5), 3783–3794, doi:10.1002/2014JA020633, 2014JA020633.

Breneman, A., A. Crew, J. Sample, D. Klumpar, A. Johnson, O. Agapitov, M. Shumko, D. Turner, O. Santolik, J. Wygant, et al. (2017), Observations directly linking relativistic electron microbursts to whistler mode chorus: Van allen probes and firebird ii, *Geophysical Research Letters*.

Crew, A. B., H. E. Spence, J. B. Blake, D. M. Klumpar, B. A. Larsen, T. P. O'Brien, S. Driscoll, M. Handley, J. Legere, S. Longworth, K. Mashburn, E. Mosleh, N. Ryhajlo, S. Smith, L. Springer, and M. Widholm (2016), First multipoint in situ observations of electron microbursts: Initial results from the nsf firebird ii mission, *Journal of Geophysical Research: Space Physics*, *121*(6), 5272–5283, doi:10.1002/2016JA022485, 2016JA022485.

Datta, S., R. Skoug, M. McCarthy, and G. Parks (1997), Modeling of microburst electron precipitation using pitch angle diffusion theory, *Journal of Geophysical Research: Space Physics*, *102*(A8), 17,325–17,333.

Dietrich, S., C. J. Rodger, M. A. Clilverd, J. Bortnik, and T. Raita (2010), Relativistic microburst storm characteristics: Combined satellite and ground-based observations, *Journal of Geophysical Research: Space Physics*, *115*(A12).

Fang, X., C. E. Randall, D. Lummerzheim, W. Wang, G. Lu, S. C. Solomon, and R. A. Frahm (2010), Parameterization of monoenergetic electron impact ionization, *Geophysical Research Letters*, *37*(22).

Gurnett, D., R. Anderson, F. Scarf, R. Fredricks, and E. Smith (1979), Initial results from the isee-1 and-2 plasma wave investigation, *Space Science Reviews*, *23*(1), 103–122.

Hoots, F. R., and R. L. Roehrich (1980), Models for propagation of norad element sets, *Tech. Rep. 3*, Spacetrack.

Horne, R. B., and R. M. Thorne (2003), Relativistic electron acceleration and precipitation during resonant interactions with whistler-mode chorus, *Geophysical Research Letters*, *30*(10), n/a–n/a, doi:10.1029/2003GL016973, 1527.

Lee, J.-J., G. K. Parks, K. W. Min, H. J. Kim, J. Park, J. Hwang, M. P. McCarthy, E. Lee, K. S. Ryu, J. T. Lim, E. S. Sim, H. W. Lee, K. I. Kang, and H. Y. Park (2005), Energy spectra of 170-360 kev electron microbursts measured by the korean stsat-1, *Geophysical*

406 *Research Letters*, *32*(13), doi:10.1029/2005GL022996, l13106.

407 Lee, J. J., G. K. Parks, E. Lee, B. T. Tsurutani, J. Hwang, K. S. Cho, K.-H. Kim, Y. D. Park,
408 K. W. Min, and M. P. McCarthy (2012), Anisotropic pitch angle distribution of 100 kev
409 microburst electrons in the loss cone: measurements from stsat-1, *Annales Geophysicae*,
410 *30*(11), 1567–1573, doi:10.5194/angeo-30-1567-2012.

411 Li, W., R. M. Thorne, V. Angelopoulos, J. Bortnik, C. M. Cully, B. Ni, O. LeContel,
412 A. Roux, U. Auster, and W. Magnes (2009), Global distribution of whistler-mode chorus
413 waves observed on the themis spacecraft, *Geophysical Research Letters*, *36*(9), n/a–n/a,
414 doi:10.1029/2009GL037595, l09104.

415 Lorentzen, K. R., J. B. Blake, U. S. Inan, and J. Bortnik (2001a), Observations of relativis-
416 tic electron microbursts in association with vlf chorus, *Journal of Geophysical Research:*
417 *Space Physics*, *106*(A4), 6017–6027, doi:10.1029/2000JA003018.

418 Lorentzen, K. R., M. D. Looper, and J. B. Blake (2001b), Relativistic electron mi-
419 crobursts during the gem storms, *Geophysical Research Letters*, *28*(13), 2573–2576, doi:
420 10.1029/2001GL012926.

421 Millan, R., and R. Thorne (2007), Review of radiation belt relativistic electron losses,
422 *Journal of Atmospheric and Solar-Terrestrial Physics*, *69*(3), 362 – 377, doi:
423 http://dx.doi.org/10.1016/j.jastp.2006.06.019, global Aspects of Magnetosphere-
424 Ionosphere CouplingGlobal Aspects of Magnetosphere-Ionosphere Coupling.

425 Millan, R. M., R. Lin, D. Smith, K. Lorentzen, and M. McCarthy (2002), X-ray observations
426 of mev electron precipitation with a balloon-borne germanium spectrometer, *Geophysical*
427 *research letters*, *29*(24).

428 Nakamura, R., D. N. Baker, J. B. Blake, S. Kanekal, B. Klecker, and D. Hovestadt (1995),
429 Relativistic electron precipitation enhancements near the outer edge of the radiation belt,
430 *Geophysical Research Letters*, *22*(9), 1129–1132, doi:10.1029/95GL00378.

431 Nakamura, R., M. Isowa, Y. Kamide, D. Baker, J. Blake, and M. Looper (2000), Observa-
432 tions of relativistic electron microbursts in association with vlf chorus, *J. Geophys. Res*,
433 *105*, 15,875–15,885.

434 O'Brien, T. P., K. R. Lorentzen, I. R. Mann, N. P. Meredith, J. B. Blake, J. F. Fennell, M. D.
435 Looper, D. K. Milling, and R. R. Anderson (2003), Energization of relativistic elec-
436 trons in the presence of ulf power and mev microbursts: Evidence for dual ulf and vlf
437 acceleration, *Journal of Geophysical Research: Space Physics*, *108*(A8), n/a–n/a, doi:
438 10.1029/2002JA009784, 1329.

O'Brien, T. P., M. D. Looper, and J. B. Blake (2004), Quantification of relativistic electron microburst losses during the gem storms, *Geophysical Research Letters*, *31*(4), n/a–n/a, doi:10.1029/2003GL018621, l04802.

Olson, W. P., and K. A. Pfitzer (1982), A dynamic model of the magnetospheric magnetic and electric fields for july 29, 1977, *Journal of Geophysical Research: Space Physics*, *87*(A8), 5943–5948, doi:10.1029/JA087iA08p05943.

Parks, G. (2003), *Physics Of Space Plasmas: An Introduction, Second Edition*, Westview Press.

Parks, G. K. (1967), Spatial characteristics of auroral-zone x-ray microbursts, *Journal of Geophysical Research*, *72*(1), 215–226.

Santolik, O., D. Gurnett, J. Pickett, M. Parrot, and N. Cornilleau-Wehrlin (2003), Spatio-temporal structure of storm-time chorus, *Journal of Geophysical Research: Space Physics*, *108*(A7).

Schulz, M., and L. J. Lanzerotti (1974), *Particle Diffusion in the Radiation Belts*, Springer.

Selesnick, R. S., J. B. Blake, and R. A. Mewaldt (2003), Atmospheric losses of radiation belt electrons, *Journal of Geophysical Research: Space Physics*, *108*(A12), doi:10.1029/2003JA010160, 1468.

Shprits, Y. Y., and R. M. Thorne (2004), Time dependent radial diffusion modeling of relativistic electrons with realistic loss rates, *Geophysical Research Letters*, *31*(8), n/a–n/a, doi:10.1029/2004GL019591, l08805.

Shprits, Y. Y., N. P. Meredith, and R. M. Thorne (2007), Parameterization of radiation belt electron loss timescales due to interactions with chorus waves, *Geophysical Research Letters*, *34*(11), n/a–n/a, doi:10.1029/2006GL029050, l111110.

Thorne, R. M. (2010), Radiation belt dynamics: The importance of wave-particle interactions, *Geophysical Research Letters*, *37*(22), doi:10.1029/2010GL044990, l22107.

Thorne, R. M., T. P. O'Brien, Y. Y. Shprits, D. Summers, and R. B. Horne (2005), Timescale for mev electron microburst loss during geomagnetic storms, *Journal of Geophysical Research: Space Physics*, *110*(A9), n/a–n/a, doi:10.1029/2004JA010882, a09202.

Tsyganenko, N. (1989), A solution of the chapman-ferraro problem for an ellipsoidal magnetopause, *Planetary and Space Science*, *37*(9), 1037 – 1046, doi:http://dx.doi.org/10.1016/0032-0633(89)90076-7.

Tsyganenko, N. A., and M. I. Sitnov (2005), Modeling the dynamics of the inner magnetosphere during strong geomagnetic storms, *Journal of Geophysical Research: Space*

Physics, *110*(A3), n/a–n/a, doi:10.1029/2004JA010798, a03208.

Ukhorskiy, A. Y., B. J. Anderson, P. C. Brandt, and N. A. Tsyganenko (2006), Storm time evolution of the outer radiation belt: Transport and losses, *Journal of Geophysical Research: Space Physics*, *111*(A11), n/a–n/a, doi:10.1029/2006JA011690, a11S03.

Woodger, L., A. Halford, R. Millan, M. McCarthy, D. Smith, G. Bowers, J. Sample, B. Anderson, and X. Liang (2015), A summary of the barrel campaigns: Technique for studying electron precipitation, *Journal of Geophysical Research: Space Physics*, *120*(6), 4922–4935.